Arab Remote Sensing and Geographic Information System Organisation

Mapping of manganese potential areas using ASTER satellite data in parts of Sultanate of Oman

Dr. Sankaran Rajendran and Dr. Sobhi Nasir

Department of Earth Sciences, Sultan Qaboos University, Al-Khod, 123 Muscat, Oman

KEYWORDS: Manganese, ASTER image processing, band ratioing, Principal Component Analysis, Wahrah Formation, Oman.

ABSTRACT

Economically viable stratiform manganese occurrences are found within the radiolarian cherts belongs to the Late Jurassic-Cretaceous age of Wahrah Formation near Ras Al Hadd region, northern east margin of Oman. In this study, their occurrence and distribution are discriminated in visible near infrared (VNIR) and short wave infrared (SWIR) multispectral bands of Advanced Spaceborne Thermal Emission and Reflection Radiometer (ASTER) using band ratio and Principal Component Analysis (PCA) image processing methods. The processed ASTER band ratio ((1 + 3)/2, (3 + 5)/4, (5 + 7)/6) image discriminated clearly the occurrence and spatial distribution of Wahrah formation in cyan colour. The RGB image of principal components PC3, PC2 and PC1 identified well the occurrences of manganese bodies in dark blue colour within the Wahrah formation of the study area. The results of image interpretations are verified in the field. The samples collected from field were studied in the laboratory using thin and polished sections under microscope and X-Ray Diffraction (XRD) analyses. This work demonstrates the sensor capability of ASTER in the mapping of manganese potential areas and the preliminary remote sensing study proposes for a large scale detailed exploration work on manganese in this region. The familiar image processing methods used in this study have great potential in the mapping of manganese bodies and associated lithology and as such are recommended for discriminating similar manganese mineralization in other arid geographic regions of the world.

INTRODUCTION

Mapping of manganese ore deposit is high economic interest. Research studies have been carried out on the occurrence, mineralogy, geochemistry and origin of manganese ores and deposits (Basta and Saleeb, 1971; Crerar et al., 1982; Devaraj and Laajoki, 1986; Peters, 1988; Kickmaier and Peters, 1990; Kickmaier, 1995; Shah and Khan, 1999; Marian et al., 2004;

Ibrahim et al., 2010) but, no adequate significant published work on the mapping of manganese potential areas using remote sensing technique, which is used as an effective tool for mapping of different lithology, ore deposits and mineral resources by several workers (Abrams et al., 1983; Crósta and Moore, 1989; Loughlin, 1991; Abrams and Hook, 1995; Rokos et al., 2000; Rowan and Mars, 2003; Crósta and Filho, 2003; Cloutis et al., 2004; Mars and Rowan, 2006; Ramadan et al., 2006; Gad and Kusky, 2007; Gabr et al., 2010; Ibrahim et al., 2010; Rajendran et al., 2011, 2012 and 2013; Rajendran and Nasir, 2013a,b). Abdeen et al. (2001) used ASTER RGB band ratios (4/7, 4/1, 2/3*4/3) and (4/7, 3/4, 2/1) for mapping of ophiolites, metasediments, volcaniclastics, and granitoids lithologic units of the Neoproterozoic Allaqi Suture in southern Eastern Desert of Egypt. Rouskov et al. (2005) used ASTER band ratios 2/1, 4/3 and 4/5 for the recognition of iron minerals versus alterations and of iron oxides in yellow to reddish colours and the alteration minerals in bluish colour in the RGB image. Hewson et al. (2006) mapped the geology associated with manganese mineralization using ASTER (multispectral) and airborne HyMap (hyperspectral) data of the Woodie Woodie manganese mineral deposits of East Pilbara. They explained that the data used allows the regional mapping of the Archaean Carawine Dolomite, which hosts Woodie Woodie style of Mn mineralisation. Gabr et al. (2010) studied the areas of high potential gold mineralization in the North-Eastern Desert of Egypt using ASTER data. They used the band ratio derived from the image spectra (4/8, 4/2 and 8/9) and linear-spectral unmixing image processing methods to extract gold related alteration minerals based on n-dimensional spectral feature space. Their results indicate that the methods are promising for the identification of alteration zones related to gold

exploration. Rajendran et al. (2011) mapped the magnetite bearing iron ore deposits from the southern Peninsular India using ASTER data. They have constructed ASTER band ratio ((1 + 3)/2, (3 + 5)/4, (5 + 7)/6) by summing the bands representing the shoulders of absorption features as a numerator and the band located nearest to the absorption feature as a denominator to map the iron ores and band ratio ((2 + 4)/3, (5 + 7)/6, (7 + 9)/8) for associated lithology of granulite terrain based on Amer et al. (2010) studied for lithological mapping of Central Eastern Desert of Egypt. Rajendran et al. (2012) discriminated the occurrences of chromite bearing mineralized zones in Semail ophiolite massifs of northern Oman Mountain using ASTER data by decorrelated stretching, band rationing and principal component analysis image processing techniques (Crósta and Moore, 1989; Loughlin, 1991; Rokos et al., 2000; Crósta and Filho, 2003; Cloutis et al., 2004; Ibrahim et al., 2010; Rajendran et al., 2012). Results of their study show that the VNIR and SWIR spectral wavelength regions are promising in detecting the areas of potential chromite bearing mineralized zones within the ophiolite region and successful for mapping of serpentinized harzburgite containing chromites. In 2013, they discriminated the hydrothermal mineralized zones and associated listwaenites in parts of Central Oman using ASTER data and band rationing, principal component analysis and the Spectral Angle Mapper (SAM) image processing techniques. The pyrolusite bearing manganese ores can be discriminated well to some extent by stretching the grey scale image of spectral bands that covers in VNIR-SWIR regions. The present work aims to detect the manganese occurrences and discriminate the potential areas in arid region using VNIR-SWIR ASTER multispectral spectral bands (rather than the expensive hyperspectral bands) and the familiar band ratios and principal component analysis image processing methods. The study is carried out on the potential occurrence of manganese bodies exposed within Wahrah Formation of Hamrat Duru group in Ras al Hadd region of the Batain basin, northeastern Oman (Fig. 1; Kickmaier and Peters, 1990).

GEOLOGICAL SETTING

The Batain plain area, one of low to moderate relief, with extensive sand and gravel cover, extends some 250 x 70 km between the Batain coast to the east and Wahiba Sands and Mastrichtian-Tertiary rocks cover to the west and north (Shackleton et al., 1990). The study area located near Ras al Hadd (22°31'30.18"N; 59°47'31.71"E) is covered mainly by two geological units namely; Hawasina Nappe and post-nappe units which consist of Tertiary and Quaternary formations (Fig. 1). The Hawasina nappe consists mainly of Hamrat Duru group rocks includes Al Jil formations (Pajv, PTRajb), Matbat Formations (TRmb1, Jmb2,), Guwayza formation (Jgw) and Wahrah formation (JKwac) of Late Permian to Callovian ages and Al Aridh group consists Sayfam formations (TRsmv, TRsm) of Triassic age. The major rock types of the formations are given in Figure 1. The Wahrah Formation is dominated by red and white radiolarian cherts and comprises a non-metamorphic sequence of fine-grained turbiditic limestones and interbedded siliceous shale. The stratiform manganese ores are occurred within the red cherts in this region and requires mapping for their occurrences in the whole northern east part of Oman (Kickmaier and Peters, 1990; Kickmaier, 1995).

The Tertiary rocks are overlying on the Hawasina nappe consist the Upper Hadhramaut group Seeb formation (Ese) of Middle Eocene age and Dhofar group Shama formation (EOsa) of Late Eocene to Oligocene ages. These formations are mainly carbonate rocks namely bioclastic limestone, marl limestone, dolomite, calcarenite and sandstone. The Quaternary rocks of the area are low active sand dunes and meso ridges (Qed), aeolian sands (Qes), slope colluviums (Qcy-z), sabkhah (Qby-z), ancient alluvial (Qtx) and sub-recent alluvial fan deposits and terraces (Qfy, Qty).

SATELLITE DATA

The ASTER sensor on board in the earth observing system (EOS) TERRA platform launched during December 1999 travels in a near circular, sun-synchronous orbit with an inclination of approximately 98.2º, an altitude of 705 km and a repeat cycle of 16 days offers relatively improved spatial, spectral, and temporal resolutions. It measures visible reflected radiation in three spectral bands (VNIR between 0.52 and 0.86 µm, with 15-m spatial resolution) and shortwave infrared radiation in six spectral bands (SWIR between 1.6 and 2.43 µm, with 30-m spatial resolution). ASTER sensor records the data in band 3B (0.76–0.86 µm) with a backward looking angle that enables the calculation of digital elevation models (DEM). In addition, it receives emitted radiation in five spectral bands in the thermal infra-red region between 8.125 and 11.65 µm, with 90-m spatial resolution (Fujisada, 1995). The increase of spectral resolution in the SWIR region (one spectral band for Landsat TM

versus four spectral bands for ASTER), enhances the surface mineralogical and lithological mapping. In the present study, the 14 ASTER Level 1B (L-1B) spectral bands date of February 02, 2006 were obtained from NASA (https://LPDAAC.usgs.gov). The data was delivered in a Tag Image File Format which provides

files for each band containing the imagery and an ASCII text .met file containing the metadata. The imagery was checked for 0% cloud cover and sensor errors, such as banding and other geometric distortions. The data were radiometric and geometric corrected and georeferenced to UTM WGS-84 projection. We chose the nine VNIR-SWIR spectral bands to process and interpret the region of interest to map the manganese occurrences as discussed above using ENVI (4.8) and ArcGIS (10.1) software's and evaluated in field and laboratory studies. The regional geological maps (Ministry of Petroleum and Minerals, 1992 and 1993) were used to verify the processed remote sensing data.

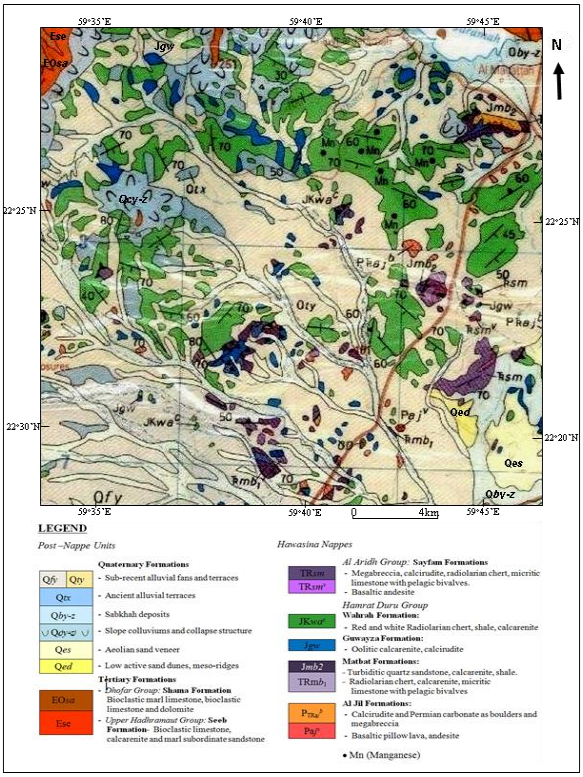

Figure 1: Geology of study region occurred near Ras Al Hadd of Al-Batain basin of NE Oman margin (Ministry of Petroleum and Minerals, 1993).

IMAGE ANALYSIS

Spectral characteristics of manganese minerals

Manganese deposits have favourable spectral absorptions characters for remote identification. The reflectance spectrum of manganese ores depends on the presence of major minerals composition of its surface, mainly pyrolusite usually a mixture of the whole rock mineralogy and weathering minerals. Comprehensive spectral absorption-compositional studies can provide important insights to the causes of spectral variations to use in the interpretation of optical remote sensing data (Cloutis et al., 2004;

Ibrahim et al., 2010 Rajendran et al, 2012 and 2013; Rajendran and Nasir, 2013). Massive manganese occurrence is a mixture of several minerals, usually with pyrolusite and psilomelane. The spectral library plot of major minerals of manganese ores such as pyrolusite (MnO2), psilomelane ((Ba, H2O)2 Mn5O10), manganite (MnO(OH)) and rhodochrosite (MnCO3) stacked from the USGS and JPL spectral libraries (Envi.4.8) are given in Figure 2.

The spectra of pyrolusite, psilomelane and manganite minerals shows spectrally featureless, quite low reflectance, strong absorption throughout the entire visible (0.3 - 0.7 µm) and reflective infrared (0.7 - 3 µm) spectral regions (Fig. 2; Hunt and Salisbury, 1971; Hunt, 1977; Clark et al., 2003; Ibrahim et al., 2010) due to the presence of predominant Mn-O molecules in its contents. The diagnostic characteristics of manganese carbonate, namely rhodochrosite (MnCO3) shows strong absorption features in the visible regions (0.3-0.7 µm) due to the Mn-O bonds and sharp absorption near 2.3 µm in the infrared region due to the C-O bonds (Abrams et al., 1988; Mars and Rowan, 2010; Rajendran and Nasir, 2013b) occurred in its contents.

The infrared spectral analyses of six samples representing the manganese ore types (manganese and manganese – iron ores) of Maliek deposits of Southern Eastern Desert, Egypt by Ibrahim et al. (2010) further confirms the absorption bands of pyrolusite and ramsdellite (MnO2) at the wave lengths of 350–400 cm−1 and 800–900 cm−1 due to metal-oxygen stretching or lattice vibrations and psilomelane absorption band at a wave length of 3,400 cm−1 due to O–H bonding.

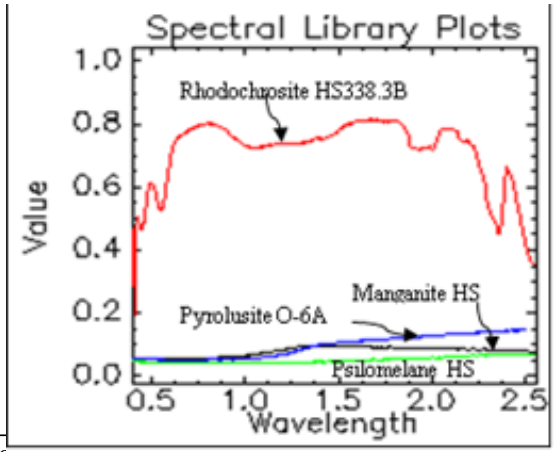

Figure 2: Spectral plot of manganese minerals stacked from USGS and JPL spectral libraries

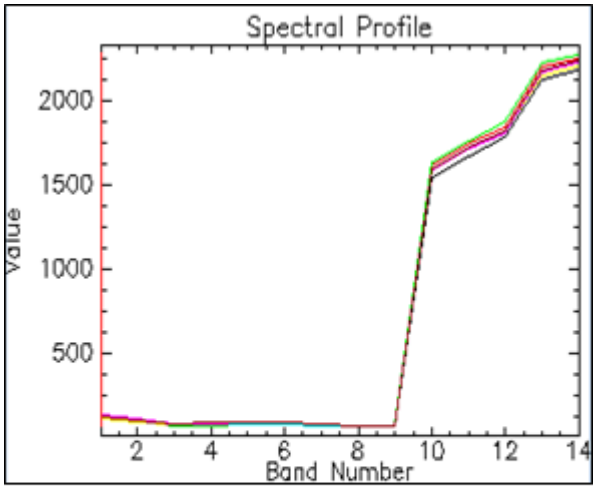

Figure 3: Image spectra of 14 ASTER spectral bands shows diagnostic absorption of manganese in VNIR and SWIR regions (1-9 spectral bands, low reflectance) and strong emission in TIR region (10-14 spectral bands).

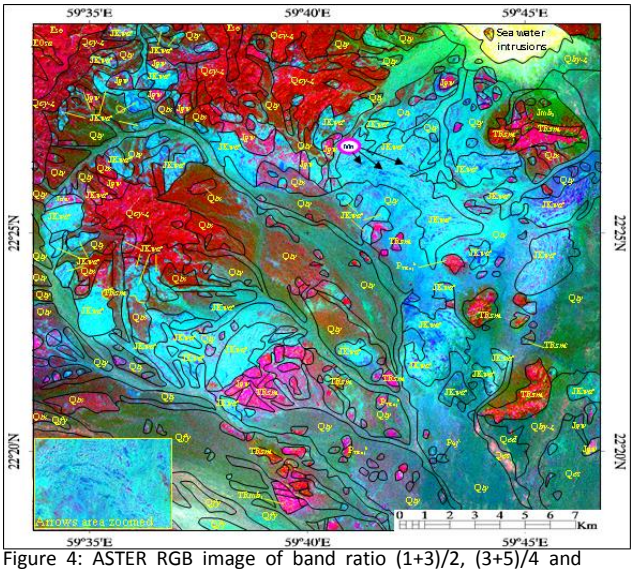

Figure 4: ASTER RGB image of band ratio (1+3)/2, (3+5)/4 and (5+7)6 of study region (legends as existed in Fig. 1).

Band Ratio

We studied the image of 14 ASTER spectral bands and collected the image spectra (Fig. 3) over the manganese occurrences (rich in pyrolusite, Peters, 1988; Kickmaier and Peters, 1990; Kickmaier, 1995) of study region, which showed the diagnostic absorption features throughout the entire VNIR and SWIR regions (in 1-9 ASTER spectral bands with low reflectance value) as described above (Fig. 2) due to the absorption of Mn-O bonds contrast to TIR region (in 10-14 ASTER spectral bands), which is more reflective due to the emission of energy from Mn-O bonds of the manganese occurrences (Rajendran and Nasir, 2013a).

The absorption found in band 12 in the image spectra is due to the contents of silica present in chert which is associated with manganese in this region (Ninomiya, 2004; Ninomiya et al., 2005).

As discussed above, based on the spectral absorptions characters of manganese minerals, we processed the 9 ASTER VNIR-SWIR spectral bands using the band ratio ((1 + 3)/2, (3 + 5)/4, (5 + 7)/6) to discriminate the occurrences of manganese and associated lithological informations. The result of analyses is given in Figure 4 (Rajendran et al., 2011).

Principal Component Analysis (PCA)

Further to confirm their occurrences, we studied the application of Principal Component Analysis on satellite data of study region. In the PCA technique, the relationship between the spectral responses of target minerals or rocks and numeric values extracted from the eigenvector matrix is used to calculate the Principal component (PC) images. Using this relationship, one can determine which PCs contain the spectral information due to the minerals and whether the digital numbers (DNs) of pixels containing the target minerals had high (bright) or low (dark) values (Crósta and Moore, 1989; Loughlin, 1991; Rokos et al., 2000; Crósta and Filho, 2003; Rajendran et al., 2012). In the PCA of 9 ASTER VNIR-SWIR spectral bands, the first three high order principal components (PC1, PC2, and PC3) have over 99% of the spectral information; hence these have been widely used for lithological mapping rather than the subsequent low order principal components (PC4, PC5, PC6, etc.) which usually contain less than 1% of spectral information and they contain low signal-to-noise ratios (Amer et al., 2010; Rajendran et al., 2012). However, some of the higher order principal components provide subtle information about the occurrence of mineral and rock types that are spatially dominant in the image (Amer et al., 2010). In this study, PCA is applied on the 9 ASTER VNIR-SWIR spectral bands (Richards and Xiuping, 1998; Rajendran et al., 2011, 2012) of study region

and the results of analyses are given in Figures 5 and 6. The pre-treatment and processing of ASTER images for above said techniques are followed as stated in Abdeen et al. (2001) and Amer et al. (2010).

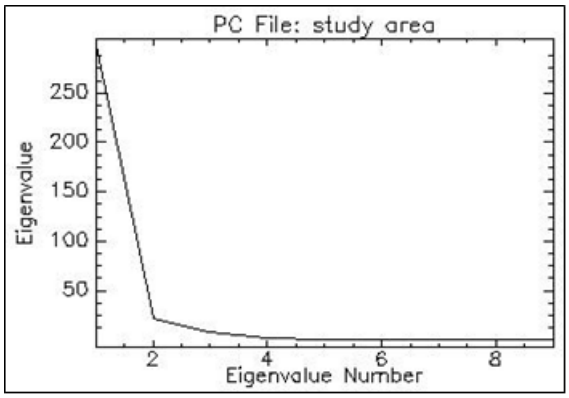

Figure 5: PCA plot shows the first few bands with maximum data and increase of noise in subsequent bands.

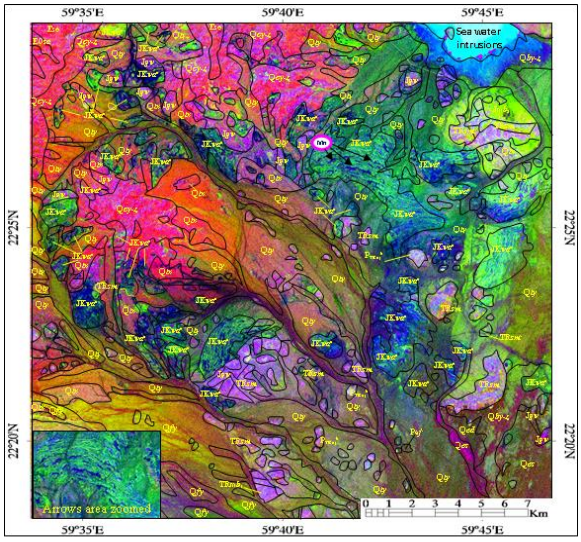

Figure 6: Principal Components RGB image (R: PC3, G: PC2 and B: PC1) of study region (legends as existed in Fig. 1).

RESULTS AND DISCUSSION

ASTER band ratio

The colour composite image formed by combining ratio bands (1 + 3)/2 in Red; ((5 + 7)/6) in Green and ((3 + 5)/4) in Blue shows valuable information on the occurrences of manganese bodies and associated lithological units and boundaries (Fig. 4) of the study region. The occurrences of manganese can be recognised by dark blue colour spotted (an example arrows marked area, zoomed part as inset) in the northern east part of study region within the Wahrah formations (JKwac) appears in cyan colour. The manganese ore appears in dark blue colour (Fig. 4) in the region is due to the strong spectral absorption of manganese minerals (Hunt and Salisbury, 1971; Hunt, 1977; Kickmaier and Peters, 1990; Clark et al., 2003; Ibrahim et al., 2010; Rajendran et al., 2011). The shades of blue and dark blue area (below the arrows marked area and in other parts) occurred within the Wahrah formations are due to the absorption of irons that are in the ferruginous red

chert of the formations. The cyan colour of Wahrah formations may be due to the presence of silica contents in the red and white radiolarian chert, shale, calcarenite and calcirudite rocks of the formations. The rocks rich in carbonate shows pink colour that can be noted in the zoomed image as pink spots within the formations. The formations are occurred as chains of small mounts and folded in the field appeared clearly on the image. The occurrences of basaltic pillow lava and andesites in Al Jil (Pajv) and Sayfam (TRsmv) formations are not discriminated well due to their minor occurrences. The other formations namely Al Jil (PTRajb), Matbat (TRmb1; Jmb2), Guwayza (Jgw) and Sayfam (TRsm) formations are discriminated by bright pink to red colours due to the presence of rich carbonates in the calcirudite, carbonate boulders, micritic limestone with pelagic bivalves, radiolarian cherts, calcarenite, turbiditic quartz sandstone and shale rocks of the formations. The formation of magabreccia (PTRajb of Al Jil and TRsm of Sayfam formations) exhibits coarse texture on the image. The Tertiary group Seeb (Ese) and Shama (EOsa) formations consists bioclasitc limestone, calcarenite, marl subordinate sandstone, bioclasitc marl limestone and dolomite rocks are appeared as dark pink to red colours due to the presence of more carbonate contents similar to the carbonate formations of Hawasina nappes. The Quaternary formations consist of alluvial sand (Qed, Qtx, Qfy and Qty), aeolian sand (Qes), and colluviums (Qcy-z) deposits show shades of dark blue to green in colours. The Sabkhah (Qby-z) formations appear in dark pink to red colours similar to Tertiary group of formations. All delineated above formations are able to study with the geology of the study region (Fig. 1). The interpretation shows that the ASTER spectral bands (having relatively high spectral spatial resolutions) and the developed ratio are capable in differentiating the Wahrah formations which contain manganese occurrences and the different lithological units of the study region.

ASTER principal component analysis

Though, the band ratio works as well in discriminating certain formations of the study region, an attempt is made to confirm their discrimination and distinguish the absorption characters of

manganese and associated rocks by correlating spectral bands and data variance through principal component analysis as discussed above. The analysis of nine ASTER VNIR-SWIR spectral bands of study region using PCA shows that the first band contains the largest percentage of data variance and the second PCA band contains the second largest data

variance, and so on; the last few PCA bands contain less than 1% of spectral information and appear noisy because they contain very little variance in the original spectral data. The first three bands are segregated with the maximum data variances over 99% of spectral informations (see spectral plot, Fig. 5). Therefore, we used the three high order principal components PC1, PC2, and PC3 for better discrimination of manganese occurrences and associated lithological units, rather than the subsequent low order principal components (4, 5, 6, etc.). The RGB image derived from the combination of PC3, PC2 and PC1 bands is given in Figure 6.

The image (Fig. 6) discriminates well almost all the formations including the Wahrah formation which consist the manganese occurrences in the region. The occurrences of manganese bodies appear clearly in dark blue colour more in the northeast part of the study region detected due to the absorption of energy by manganese bearing minerals that occurred within the cherts of Wahrah formations which appears in shades of green colours due to the presence of rich silica in red and brown cherts (see inset in Figure 7). The shades of blue and dark blue area (below the arrows marked area and in other parts) occurred within the Wahrah formations are due to the absorption of irons that are in the ferrugenous red chert of the formations. The occurrence of manganese, in dark blue colour within the shades of green colour, can be distinguished from the shades of blue colour that represent the ferrugenous cherts. The other formations of Hamrat Duru group consists of red and white radiolarian cherts, shale, quartz sandstone, micritic limestone with pelagic bivalves, calcarenite and calcirudite rocks appear in purple or shades of purple in colours due to presence of silica, silicates and carbonates. The Tertiary group formations are shown in dark pink to red in colours. The Quaternary formations appears in orange to the shades of light green colours. The Sabkhah formations appear in dark pink to red colours similar to Tertiary group of formations. The interpretations show clearly the occurrences of manganese ores and the analyses better discriminated the rock units those associated with manganese bodies, the manganese potential areas of the study region. The principal component analysis (RGB image of PC3, PC2, and PC1; Fig. 6) is proved powerful in discriminating the occurrences of manganese ore in Wahrah formations and the associated rock units of the study region. The results obtained from the ASTER band ratios and PCA images are verified in the field and studied in the laboratory as discussed in the following section 6.

Field and laboratory studies

Systematic field verifications are carried out on the occurrences of manganese ores and associated rock formations discriminated on the image by difference in tones and are verified at several locations for their occurrences, distributions and contacts and traverse based samples were collected during May, 2012 near Ras Al Hadd region. The importance is given to manganese ore occurrences and associated cherts of Wahrah formation of Hamrat Duru group. In field, the occurrences of stratiform manganese ores within the cherts of Wahrah Formation (Figs. 7a, b) are confirmed. The cherts mainly consists of ribbon radiolarian cherts and siliceous clay interbeds exposed continuously over several hundred meters as chain of hills with the occurrences of manganese ores along strike in vertical sequences (Fig. 7a). Their occurrences can be classified into (i) brown cherts (with homogeneous distribution of Mn, Fig. 7c); (ii) laminated cherts (with enrichment of Mn particles to fine laminae in variable thickness 0.01-0.2 cm), (iii) layered Mn-cherts (with Mn enrichment to layers thicker than 0.2 cm, Fig. 7a); (iv) black siliceous cherts (dark brown to black Mn rich cherts, Fig. 7d); (v) nodular Mn-aggregates in red cherts (with elliptical or oval nodules of variable size <1-8 cm, Fig. 7e) as studied by Kickmaier (1995) and Kickmaier and Peters (1990). Large scale enrichment of manganese is observed in the folded horizon (see insets of Figures 4 and 6). The manganese horizon starts from brown cherts to manganese-layered cherts and high manganese-rich black siliceous cherts are occurred at the center of the sequence (Figs. 7f, g). The occurrence of highly weathered and fragmented ferrugenous red cherts and developed iron residues in and around of formations are also observed (insets in Figure 7a). In field, the manganese appears as gray-white and show metallic lustre, brittleness, small nodular segregations (Fig. 7d) and concentrated as pyrolusite mineral masses (Fig. 7g) with negligible amount of iron minerals. The layers are parallel to the bedding of cherts (Fig. 7g) but have an irregular surface. The chert layers occurred within the massive manganese is typically black in colour, more or less homogeneous fine texture and

shows the presence of fine manganese laminae (Fig. 7g). Occasionally, the black part of the chert is bounded by intense brown chert. The occurrences of nodular-shaped manganese-segregations are found in muddy cherts. These are slightly elongated and parallel to bedding (Fig. 7e). The occurrence of manganese is also found associated with carbonatite observed at few places within the cherts of Wahrah formation (Fig. 7h; Nasir et al., 2011).

The polished surface of Mn-rich cherts of the region shows homogeneous distribution of fine grained manganese-segregations (pyrolusite, 2mm to 7mm in sizes) and can be unambiguously determined in black siliceous cherts (i.e. as disseminated, Fig. 8a). No sharp contacts between the manganese-rich laminae and the chert with disseminated manganese were observed. The manganese-layer consists of amorphous pyrolusite and microcrystalline chalcedonic quartz. Microscopic thin section study shows the presence of pyrolusite as the principal manganese mineral. It has high reflectivity (Fig. 8b), distinct bireflection and strong anisotropic characters (Figs. 8c, d; Ibrahim et al., 2010). Pyrolusites exhibit as well-crystallized euhedral prismatic or spindle shaped crystals and are radially distributed (Fig. 8d). The presence of cryptomelanes are found in gray colour, varying from dull gray to bright gray colours, commonly occurred as concentric rhythmic bands with concavo-convex surfaces and show mammillary botryoides giving rise colloform textures (Fig. 8c; Ibrahim et al., 2010). These are medium to high reflectivity and weak anisotropism. The accessory minerals namely calcite, quartz, apatite and chlorite are observed. Quartz occurs as veinlets and well-developed crystals crushed due to deformation. Apatite is found as rod-like grains with high relief and parallel extinction scattered within manganese matrix. Chlorites found as fibrous grains showed blue interference colour in the ore minerals.

The samples collected from the field are analyzed by the X-Ray powder Diffraction (XRD) method to evaluate the occurrence of manganese minerals of the region. The results of selected XRD analyses are given in Figure 9, which confirms the presence of major manganese minerals such as pyrolusite and cryptomelane (Figs. 9a, b) in the samples. The occurrences of manganite are also evidenced in the analyses. In laboratory, the heating of manganese (mineral pyrolusite - manganese dioxide) is formed a charcoal fire. The heat and carbon in the charcoal separated oxygen from the pyrolusite, leaving a metallic manganese residue.

The mineralogical, geochemical and sedimentalogical characters of similar stratiform manganese of the Wahrah Formations of Ras Al Hadd and Al Hammah regions are studied by Peters (1988), Kickmaier and Peters (1990), and Kickmaier (1995). Literature review shows that Mn bodies are characterized by the presence of high Mn, extreme Mn/Fe ratios and by low minor element (e.g. Ni, Cu, Co) contents (Kickmaier, 1995) which are the supportive

evidences of the strong spectral absorptions (dark blue) on the image interpretations. The minimum and maximum values of selected major and minor elemental chemical composition of Mn bodies of Ras Al Hadd and Mn-rich cherts of Al Hammah regions (Kickmaier, 1995) are given in Table 1.

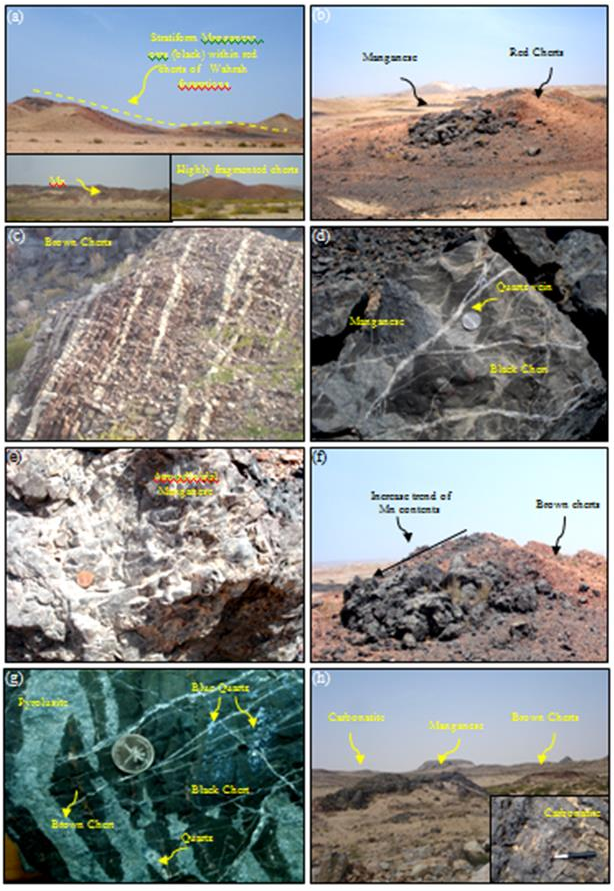

Figure 7: Field photographs (Location M in Figs. 4 and 6) shows a. and b. stratiform manganese occurrences within red cherts, c. the brown cherts interbedded with siliceous clay, d. the black siliceous cherts with Mn occurrences e. the nodular Mn-aggregates in red cherts, f. the occurrence of manganese at the center of brown cherts, g. the Mn layers are parallel to the bedding of cherts and h. the Mn and carbonatite occurrences within Wahrah Formation.

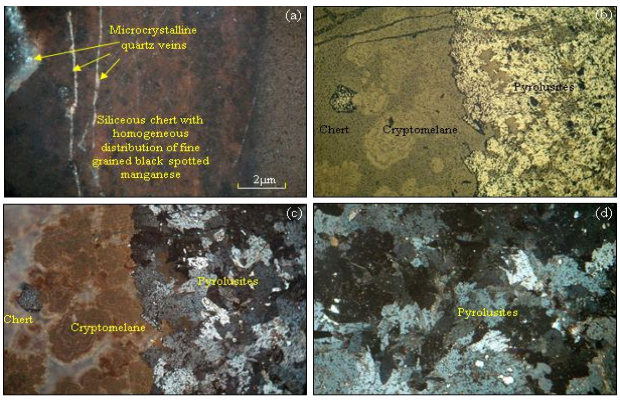

Figure 8: a. The polished sample of Mn-rich chert shows the occurrence of fine grained manganese and microcrystalline quartz vein, b. the microphotographs shows the occurrence of pyrolusite,

cryptomelane and chert under the nicols parallel and (25 x), c. under the nicols crossed (25 x) and d. the occurrence of prismatic and spindle shaped pyrolusite (nicols crossed, 35 x) in massive ore.

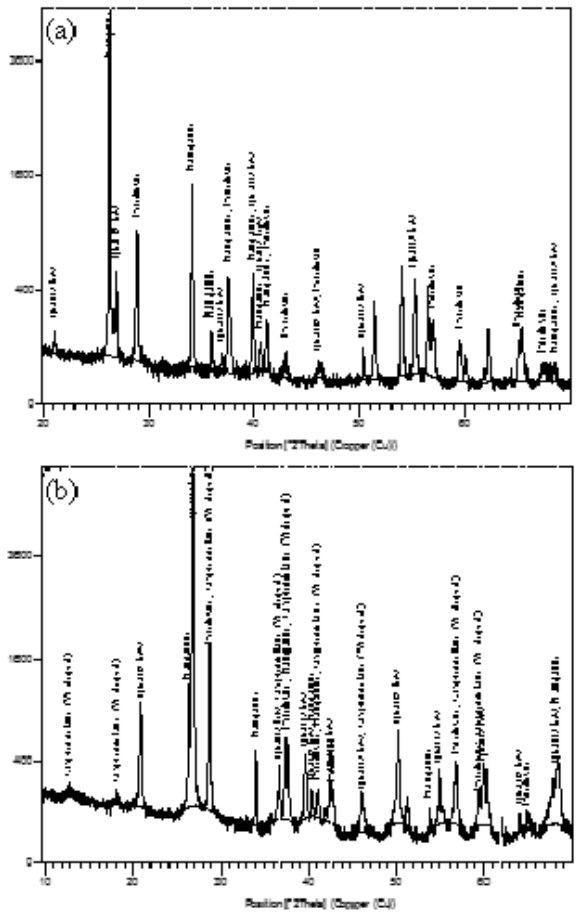

Figure 9: XRD analyses a. and b. shows the presence of pyrolusite, cryptomelane and manganite minerals in the samples of study region.

Elements	Major Elements [§]				Trace elements[*]				
	Mn	Fe	Mn/Fe	SiO_2	Co	Cr	Cu	Ni	Zn
Mn bodies of Ras Al Hadd	3.64 - 54.20	0.1 -0.9	8.5 – 542.0	3.58 – 88.07	18 - 91	5 – 618	68 - 133	15 – 166	11 – 142
Mn-rich cherts of Al Hammah	1.24 – 39.60	1.09 – 0.08	1.0 – 360.0	47.72 – 92.59	18 – 132	11 – 337	12 – 619	15 – 388	12 - 93

Table 1: The minimum and maximum values of selected major and minor elements chemical composition of Mn ore bodies of Ras Al Hadd region and Mn-rich cherts of Al Hammah region (Kickmaier, 1995).

CONCLUSION

In this study, the occurrences of manganese ores and associated lithological formations found near Ras Al Hadd region of Batain basin are discriminated in VNIR-SWIR ASTER spectral bands by the band ratio ((1 + 3)/2, (3 + 5)/4, (5 + 7)/6) and Principal Component Analysis (PC3, PC2, and PC1) image processing methods and interpreted. The interpretations of manganese ores and associated

rocks over the processed image are verified through field and laboratory studies and proved that the applied methods are successful. The studied techniques are time- and cost-effective in the mapping of manganese occurrences and associated formations and thus we recommend to use the techniques in the arid region anywhere in the world. Moreover, this work demonstrates the sensor capability of ASTER in providing informations on the occurrences of manganese, which is valuable for mineral prospecting and exploration activities. The preliminary remote sensing study recommends for a large scale detailed exploration work on the occurrences of manganese in this region.

Acknowledgements

The authors are thankful to NASA Land Processes Distributed Active Archive Center User Services, USGS Earth Resources Observation and Science (EROS) Center https://LPDAAC.usgs.gov) for providing the ASTER data. The XRD analytical help extended by Mr. Saif Amer Al-Maamari, and the preparation of micro thin sections by Mr. Hamdan Saif Al-Zidi, Department of Earth Sciences, Sultan Qaboos University are thankfully acknowledged.

References

Abdeen, M.M., Allison, T.K., Abdelsalam, M.G., Stern, R.J., 2001. Application of ASTER band-ratio images for geological mapping in arid regions: The Neoproterozoic Allaqi suture, Egypt. Geological Society of America Annual Meeting, Abstracts with Programs, Boston, USA, November 5-8, 2001 33 (6), 123

Abrams, M.J., Brown, D., Lepley, L., Sadowski, R., 1983. Remote sensing for porphyry copper deposits in southern Arizona. Economic Geology 78, 591–604.

Abrams, M.J., Hook, S.J., 1995. Simulated ASTER data for geologic studies. IEEE Transactions of Geoscience and Remote Sensing 33, 692–699.

Abrams, M.J., Rothery, D.A., Pontual, A., 1988. Mapping in the Oman Ophiolite using enhanced Landsat Thematic Mapper images. Tectonophysics 151, 387–401.

Amer, R., Kusky, T.M., Ghulam, A., 2010. New methods of processing ASTER data for lithological mapping: examples from Fawakhir, Central Eastern Desert of Egypt. J. Afr. Earth Sci. 56 (2–3), 75–82.

Basta, E.Z., Saleeb, W. S., 1971. Elba manganese ores and their origin, South-eastern Desert, U.A.R. Mineralogical magazine 38, 235-244.

Clark, R. N., Swayze, G. A., Wise, R., Livo, K. E., Hoefen, T. M., Kokaly, R. F., Sutley, S. J., 2003. USGS Digital Spectral Library splib05a. U.S. Geological Survey, Open File Report 03-395.

Cloutis, E.A., Sunshine, J. M., Morris, R. V., 2004. Spectral reflectance-compositional properties of spinels and chromites: Implications for planetary remote sensing and geothermometry. Meteoritics and Planetary Science 39(4), 545–565.

Crerar, D. A., Namson, J., So Chy, M., Williams, L., Feicenson, M. D., 1982. Manganiferous cherts of the Franciscan assemblage: I. General Geology, Ancient and modern analogues, and implications for hydrothermal convection at oceanic spreading centers. Economic Geology 77/3, 519-540.

Crósta, A.P., Moore, M.J., 1989. Enhancement of Landsat Thematic Mapper imagery for residual soil mapping in SW Minas Gerais State Brazil: a prospecting case history in greenstone belt terrain. 9th Thematic Conference on Remote Sensing for Exploration Geology, Environmental Research Institute of Michigan, Ann Arbor. 1173–1187.

Crósta, A.P., Filho, C.R.d.S., 2003. Searching for gold with ASTER. Earth Observation Magazine 12 (5), 38–41.

Devaraj T.C., Laajoki., 1986. Mineralogy and mineral chemistry of the manganese-poor and manganiferous iron-formations from the high-grade metamorphic terrain of Southern Karnataka, India. Journal of Geological Society of India 28, 134-164.

Fujisada, H., 1995. Design and performance of ASTER instrument. Proceedings of SPIE, The International Society for Optical Engineering 2583, 16–25.

Gabr, S., Ghulam, A., Kusky, T., 2010. Detecting areas of high-potential gold mineralization using ASTER data. Ore Geology Reviews 38, 59–69.

Gad, S., Kusky, T.M., 2007. ASTER spectral ratioing for lithological mapping in the Arabian-Nubian shield, the Neoproterozoic Wadi Kid area, Sinai, Egypt. Gondwana Research 11 (3), 326–335.

Hunt, G.R., Salisbury, J. W., 1971. Visible and near-infrared spectra of minerals and rocks: II. Carbonates. Modern Geology v2, 23-30.

Hunt, G. R., 1977. Spectral signatures of particulate minerals in the visible and near infrared. Geophysics 42, 501-513.

Ibrahim, A., Salem Mohamed E. Ibrahim., Mohamed Abd El Monsef., 2010. Mineralogy, geochemistry, and origin of hydrothermal manganese veins at Wadi Maliek, Southern Eastern Desert, Egypt. Arab J Geosci. DOI 10.1007/s12517-010-0195-1.

Kickmaier, W., Peters, Tj., 1990. Manganese occurrences in the A1 Hammah Range – Wahrah Formation, Oman Mountains. Geological Society Special Publication 49, 239-249

Kickmaier, W., 1995. Chert hosted Manganese deposits in the Wahrah Formation, A1 Hammah Range, Sultanate of Oman. Report of Ministy of Petroleum and Minerals 168 pp.

Loughlin, W.P., 1991., Principal component analysis for alteration mapping. Photogrammetric Engineering and Remote Sensing 57, 1163–1169.

Marian Munteanu., Stefan Marincea., Haino Uwe Kasper., Karel Zak., Veronica Alexe., Vasile Trandafir., George Saptefrati., Angela Mihalache., 2004. Black chert-hosted manganese deposits from the Bistritei Mountains, Eastern Carpathians (Romania): petrography, genesis and metamorphic evolution. Ore Geology Reviews 24, 45–65.

Mars, J.C., Rowan, L.C., 2006. Regional mapping of phyllic- and argillic-altered rocks in the Zagros magmatic arc, Iran, using Advanced Spaceborne Thermal Emission and Reflection Radiometer (ASTER) data and logical operator algorithms. Geosphere 2 (3), 161–186.

Mars J.C., Rowan L.C., 2010. Spectral assessment of new ASTER SWIR surface reflectance data products for spectroscopic mapping of rocks and minerals. Remote Sensing of Environment 114, 2011–2025.

Nasir, S., Al-Khirbash, S., Rollinson, H., Al-Harthy, A., Al-Sayigh, A., Al-Lazki, A., Theye, T., Massonne, H. J., Belousova, E., 2011. Petrogenesis of early cretaceous carbonatite and ultramafic lamprophyres in a diatreme in the Batain Nappes, Eastern Oman continental margin. Contribution to Mineralogy and Petrology 161, 47–74.

Ninomiya, Y., 2004. Lithologic mapping with multispectral ASTER TIR and SWIR data. P SPIE 5234, 180-190.

Ninomiya, Y., Fu, B., Cudahy, T. J., 2005. Detecting lithology with Advanced Spaceborne Thermal Emission and Reflection Radiometer (ASTER) multispectral thermal infared “radiance-at-sensor” data. Remote Sens. Environ. 99, 127-139.

Peters, Tj., 1988. Geochemistry of manganese-bearing cherts associated with Alpine ophiolites and the Hawasina formations in Oman, Marine Geology 84(3–4), 229–238.

Rajendran, S., Nasir, S., Kusky, T.M., Ghulam, A., Gabr, S., El Gali, M., 2013. Detection of hydrothermal mineralized zones associated with Listwaenites rocks in Central Oman using ASTER data. Ore Geology Reviews 53, 470–488.

Rajendran, S., Nasir, S., 2013b. ASTER mapping of limestone formations and study of caves, springs and depressions in parts of Sultanate of Oman. Environ Earth Sci. DOI 10.1007/s12665-013-2419-7.

Rajendran, S., Nasir, S., 2013a. ASTER spectral analysis of ultramafic lamprophyres (carbonatites and aillikites) within the Batain nappe, northeastern margin of Oman - A proposal developed for Spectral Absorption. International Journal of Remote sensing 34(8), 2763–2795.

Rajendran, S., Al-Khirbash, S., Pracejus, B., Nasir, S., Al-Abri, A.H., Kusky, T.M., Ghulam, A., 2012. ASTER detection of chromite bearing mineralized zones in Semail Ophiolite Massifs of the northern Oman mountain: Exploration strategy. Ore geology reviews 44, 121-135.

Rajendran, S., Thirunavukkarasu, A., Balamurugan, G., Shankar, K., 2011. Discrimination of Iron Ore Deposits of Granulite Terrain of Southern Peninsular India using ASTER data. Journal of Asian Earth Sciences 41, 99–106.

Ramadan, T.M., Nasr, A.H., Mahmood, A., 2006. Integration of Radarsat-1 and Landsat TM images for mineral exploration in East Oweinat District, South Western Desert, Egypt. ISPRS Commission VII Mid-term Symposium "Remote Sensing: From Pixels to Processes", Enschede, The Netherlands, May 8-11, 2006 244-249.

chards, J.A., Xiuping, J., 1998. Remote Sensing Digital Image Analysis. Third ed. Springer, Berlin 363 pp.

Rokos, D., Argialas, D., Mavrantza, R., St.-Seymour, K., Vamvoukakis, C., Kouli, M., Lamera, S., Paraskevas, H., Karfakis, I., Denes, G., 2000. Structural mapping and analysis for a preliminary investigation of possible gold mineralization by using remote sensing and geochemical techniques in a GIS environment: study area: island of Lesvos, Aegean Sea, Hellas. Natural Resources Research 9, 277–293.

Rouskov, K., Popov, K., Stoykov, S., Yamaguchi, Y., 2005. Some applications of the remote sensing in geology by using of ASTER images. Scientific Conference “Space, Ecology, Safety”, Varna, Bulgaria, 10–13 June 2005 167-173.

Rowan, L.C., Mars, J.C., 2003. Lithologic mapping in the Mountain Pass, California area using Advanced Spaceborne Thermal Emission and Reflection Radiometer (ASTER) data. Remote Sensing of Environment 84 (3), 350–366.

Shackleton, R.M., Ries. A. C., Bir. P. R., Filbrandt. J. B., Lee. C. W., Cunningham. G. C., 1990. The Batain Melange of NE Oman. Geological Society Special Publication 49, 673-696.

Shah, M.T., Khan, A., 1999. Geochemistry and origin of Mn-deposits in the Waziristan ophiolite complex, North Waziristan. Pakistan.Miner Deposita 34, 697–704.